

A calibration of the mixing-length for solar-type stars based on hydrodynamical simulations

I. Methodical aspects and results for solar metallicity

Hans-Günter Ludwig¹, Bernd Freytag^{1,2}, and Matthias Steffen^{3,2}

¹ Astronomical Observatory, Juliane Maries Vej 30, DK-2100 Copenhagen Ø, Denmark [hgl@astro.ku.dk, bf@astro.ku.dk]

² Institut für Theoretische Physik und Astrophysik der Universität Kiel, D-24098 Kiel, Germany

³ Astrophysikalisches Institut Potsdam, D-14482 Potsdam, Germany, [MSteffen@aip.de]

Received 28 September 1998; accepted date

Abstract. Based on detailed 2D numerical radiation hydrodynamics (RHD) calculations of time-dependent compressible convection, we have studied the dynamics and thermal structure of the convective surface layers of solar-type stars. The RHD models provide information about the convective efficiency in the superadiabatic region at the top of convective envelopes and predict the asymptotic value of the entropy of the deep, adiabatically stratified layers (Fig. 3). This information is translated into an effective mixing-length parameter α_{MLT} suitable to construct standard stellar structure models. We validate the approach by a detailed comparison to helioseismic data.

The grid of RHD models for solar metallicity comprises 58 simulation runs with a helium abundance of $Y = 0.28$ in the range of effective temperatures $4300 \text{ K} \leq T_{\text{eff}} \leq 7100 \text{ K}$ and gravities $2.54 \leq \log g \leq 4.74$. We find a moderate, nevertheless significant variation of α_{MLT} between about 1.3 for F-dwarfs and 1.75 for K-subgiants with a dominant dependence on T_{eff} (Fig. 5). In the close neighbourhood of the Sun we find a plateau where α_{MLT} remains almost constant. The internal accuracy of the calibration of α_{MLT} is estimated to be ± 0.05 with a possible systematic bias towards lower values. An analogous calibration of the convection theory of Canuto & Mazzitelli (1991, 1992; CMT) gives a different temperature dependence but a similar variation of the free parameter (Fig. 6).

For the first time, values for the gravity-darkening exponent β are derived independently of mixing-length theory: $\beta = 0.07 \dots 0.10$.

We show that our findings are consistent with constraints from stellar stability considerations and provide compact fitting formulae for the calibrations.

Key words: convection – hydrodynamics – stars: late-type – stars: evolution

1. Introduction

The structure and evolution of late-type stars is intimately related to convective transport processes taking place in their outer envelopes. Although the underlying physical principles are well known, the non-linear and non-local character of the equations describing the convective motions in a radiating, partially ionized fluid has hampered the development of a closed analytical theory. Hitherto standard stellar structure models include the convective energy transport in the framework of mixing-length theory (MLT). Despite its heuristic nature MLT has proven to be rather successful and is still the working horse in stellar structure modeling. During recent years much effort has been put into the refinement of the theoretical description of microphysical stellar plasma properties — the opacity and the equation of state. To fully benefit from these improvements, an accompanying development of the description of hydrodynamical transport properties appears to be necessary, in the first place aiming at a better understanding of the convective energy transport. In this paper we report on such an effort relying on direct numerical simulations of convective flows in solar-type stars.

Primarily due to the heavy demands on computational resources, RHD simulations have concentrated very much on the Sun, and only rather few models have been constructed for other objects (Nordlund 1982, Steffen et al. 1989, Nordlund & Dravins 1990, Ludwig et al. 1994, Freytag et al. 1996). This sparseness has prevented a broader application of results of RHD simulations to the modeling of stellar atmospheres and evolution. We try to overcome this limitation in this work by computing a *grid of RHD models*, allowing a systematic study of the characteristics of convective flows in a larger region of the Hertzsprung-Russell diagram (HRD). We point out that the RHD simulations have now reached a level of sophistication far beyond idealized, simple numerical experiments. We consider it an important aspect of our work that it presents a *quantitative study* and — as such — puts emphasis on the estimation of the achieved accuracy. Aiming at an application in the field of stellar evolution, we concentrate on the evaluation of one struc-

tural quantity, namely the entropy of the adiabatically stratified layers deep in the convective stellar envelope. In the following we shall refer to this entropy as s_{env} . Its relevance for stellar structure stems from the fact that it strongly influences the radius of a star. To obtain handy numbers, all entropy values in this paper — unless stated otherwise — are given in units of $s_0 = 10^9$ erg/g/K. To link our results more directly to standard stellar structure modeling we translate s_{env} into an equivalent mixing-length parameter.

Some words concerning our nomenclature: we use the term “solar-type” for stars with extended convective envelopes where the thickness of the superadiabatic layers at the top of this envelope is small in comparison to the stellar radius. “Grey” radiative transfer means that frequency-independent (mean) opacities were used in the computation of the radiation field. The opacities still depend on temperature and density and include contributions from spectral lines.

In the paper we proceed as follows: we start with methodical aspects describing our hydrodynamical models, the basic idea and the procedure to derive s_{env} , and the translation of s_{env} into an equivalent mixing-length. We continue with the validation of our method by showing that we are able to predict the solar structure derived from helioseismic measurements within small uncertainties. We then present the calibrations of MLT and CMT. We discuss the application of our results to stellar modeling, point out consequences of stellar stability considerations, present a derivation of the gravity-darkening exponent, and contrast our approach with others. We conclude with future perspectives. In the appendix we provide some auxiliary data helping to utilize our findings in stellar structure models.

2. Methodical aspects

2.1. Hydrodynamical models of solar-type surface convection

We have obtained detailed 2-dimensional models of the surface layers of solar-type stars from extensive numerical simulations solving the time-dependent, non-linear equations of hydrodynamics for a stratified compressible fluid. The calculations take into account a realistic equation-of-state (EOS, including the ionization of H and He as well as formation of H₂-molecules) and use an elaborate scheme to describe multi-dimensional, non-local, frequency-dependent radiative transfer. Similar to classical model atmospheres, the hydrodynamical models are characterized by effective temperature T_{eff} , acceleration of gravity $\log g$, and chemical composition. They include the photosphere as well as part of the subphotospheric layers, with an *open lower boundary*, allowing a free flow of gas out of and into the model. A fixed specific entropy s^* is (asymptotically) assigned to the gas entering the simulation volume from below. The value adopted for s^* uniquely determines the effective temperature of the hydrodynamical model. For details about the physical assumptions, numerical method and characteristics of the resulting convective flows see Ludwig et al. (1994) and Freytag et al. (1996).

2.2. From the surface to the base of a convection zone

Figure 1a shows the *mean* entropy as a function of depth obtained from a hydrodynamical granulation model of the Sun by averaging over horizontal planes and over time. As in this example, our models in general do not extend deep enough to include those layers where the mean stratification of the convection zone becomes adiabatic. While the mean entropy stratification of the hydrodynamical models does not permit a direct determination of the entropy corresponding to the adiabat of the deep convection zone, the *spatially resolved* entropy profiles contain additional information. Figure 1b displays the entropy profiles for an arbitrary instant of the sequence from which the mean stratification in Fig. 1a was computed. The granular convection pattern at the surface of solar-type stars is formed by broad hot upflows accompanied by concentrated cool downdrafts. Figure 1b shows a remarkable entropy plateau in the subsurface layers, indicating that — in contrast to the narrow downdrafts — the gas in the central regions of the broad ascending flows is still thermally isolated from its surroundings. Neither radiative losses nor entrainment by material of low entropy can produce significant deviations from adiabatic expansion until immediately below the radiating surface layers. The height of the entropy plateau is essentially independent of time and corresponds to s^* .

We suggest that s^* may be identified directly with the entropy s_{env} of the deep, adiabatic convective layers:

$$s_{\text{env}} = s^*. \quad (1)$$

This idea has been put forward by Steffen (1993) and Ludwig et al. (1997) and is based on the qualitative picture of solar-type convection zones proposed by Stein & Nordlund (1989) (hereafter referred to as “SN scenario”) which is fundamentally different from MLT assumptions. According to this scenario the downdrafts continue all the way from the surface to the bottom of the convection zone, merging into fewer and stronger currents at successively deeper levels. The flow closes only near the base of the convective envelope. Most of the gas elements starting from the bottom of a deep convection zone overturn into neighbouring downflows before reaching the surface. Only a very small fraction of gas continues to the surface, reaching the layers corresponding to the location of the lower boundary of our hydrodynamical models essentially without entropy losses, following an adiabat almost up to the visible surface. Hence, s^* obtained from the simulations is the entropy of the warm, ascending gas throughout the convection zone. This, in turn, is very nearly equal to the mean (horizontally averaged) entropy s_{env} near the base of the convection zone because (i) the downflows are markedly entropy-deficient only near the surface and become continuously diluted by overturning entropy-neutral gas as they reach greater depths, and (ii) the fractional area occupied by the downdrafts decreases with depth.

We note that for this investigation it is actually irrelevant whether the downflows possess a plume-like character or take

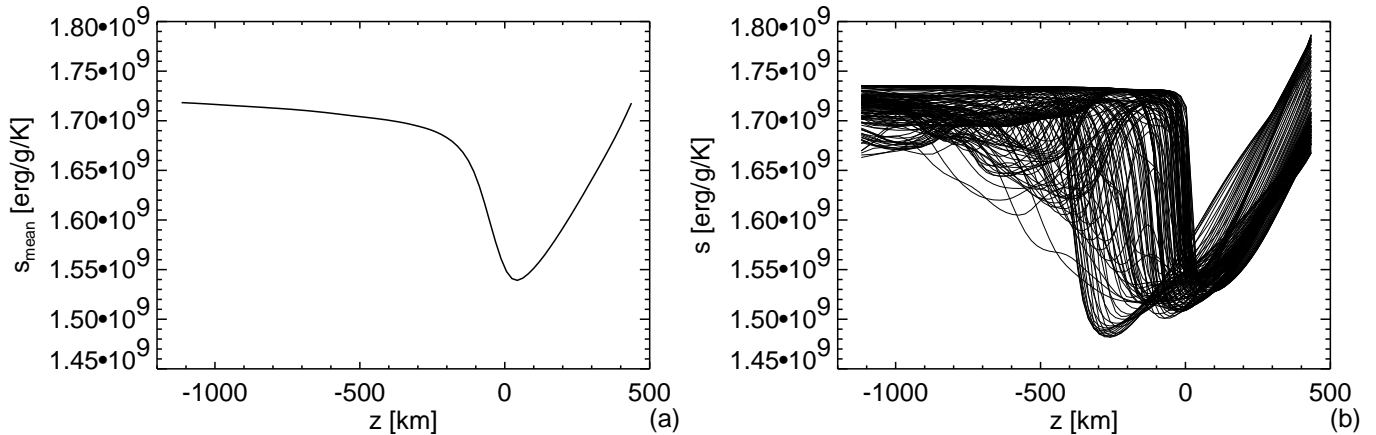


Fig. 1. Depth dependence of the entropy in the solar surface layers as obtained from hydrodynamical simulations ($T_{\text{eff}} = 5770$ K, $\log g = 4.44$, model code L71D07) performed on a 140 (x) by 71 (z) grid with frequency-dependent radiative transfer. The mean entropy (horizontal and temporal average) is shown in panel (a), spatially resolved entropy profiles in panel (b). Geometrical height zero corresponds to $\tau_{\text{Ross}} = 1$. Note that the model comprises only the uppermost part of the 200 Mm deep solar convective zone.

place in another form. The essential point is that sinking material does not locally affect the entropy of rising material by draining heat from it. The role of the downflows is reduced to a dynamical one: while sinking downwards they simply displace buoyancy-neutral material and push it upwards.

2.3. Functional dependence of s_{env} on stellar parameters

When considering the MLT picture and the SN scenario it is interesting to ask what stellar properties determine s_{env} or — in other words — what coordinates are appropriate to describe its functional dependence in the HRD. We argued that hydrodynamical models of the surface layers are able to provide information about s_{env} . The models are characterized by the *atmospheric parameters* and consequently we describe s_{env} in terms of them. Whether the standard atmospheric parameters T_{eff} and $\log g$ are the most suitable coordinates is not clear. One might speculate that e.g. the surface opacity is a physically more relevant quantity. Nevertheless, for solar-type stars the conditions at the stellar surface govern the global envelope structure and the standard atmospheric parameters are suitable coordinates to parameterize them. They have the advantage that they are external control parameters and not part of the solution of the problem. For solar-type stars with superadiabatic regions which are thin in comparison to the stellar radius we expect the same qualitative behaviour irrespective of whether we consider the MLT picture or the SN scenario. Global stellar parameters (mass, radius, or age) play only an indirect role for the entropy jump. The situation changes when the size of the granular cells or the thickness of the superadiabatic layer become comparable to the stellar radius. This might happen in giants and one has to account for effects introduced by the global stellar structure, i.e. sphericity effects.

2.4. α_{MLT} from envelope models

Although s_{env} allows the construction of the envelope structure with the necessary precision, it is of interest to translate this quantity to an equivalent α_{MLT} since this parameter is conventionally used in stellar structure models. For this purpose we computed grids of standard stellar envelope models (not subject to central boundary conditions) based on MLT, covering the relevant range of effective temperature and gravity and assuming $Y = 0.28$ and solar metallicity for the chemical composition. In these models α_{MLT} was a free parameter. For given stellar parameters (T_{eff} , $\log g$) we obtained s_{env} as a function of α_{MLT} . By matching s_{env} from the RHD models we deduced the corresponding α_{MLT} . Figure 2 illustrates this procedure for a number of representative models. Each panel shows the entropy profile of the envelope model matching s_{env} from a RHD simulation. For comparison two further envelope models are plotted with α_{MLT} varied by ± 0.05 with respect to the matching one, as well as an estimate of the uncertainty of s_{env} stemming from the temporal fluctuations of s^* which we observe during the simulation run. Although at first glance the matching is a straightforward procedure, it is important to take care of a number of fine points in order to ensure a unique and well-defined calibration of α_{MLT} . We discuss these points in the following.

Concerning the *opacities* and *EOS* we tried to stay as close as possible to the physical description used in the RHD models. Due to this differential procedure, systematic uncertainties are substantially reduced. In the RHD models ATLAS6 opacities according Kurucz (1979) are adopted. These opacities contain no contribution from molecular lines. Since the envelope models reach much deeper than the RHD models we supplemented the ATLAS6 opacities by OPAL opacities for higher temperatures (Rogers & Iglesias 1992). Care was taken that the chemical mixture assumed in both data sets was as similar as possi-

ble. In the envelope models we used the RHD EOS throughout. It is a simple EOS taking into account the ionization equilibria of hydrogen and helium according to the Saha-Boltzmann equations.

The RHD EOS has the advantage of great smoothness and computational efficiency. It might appear that this description is too crude, especially for the envelopes of cooler objects where non-ideal effects become more pronounced. However, this simplification is tolerable since the entropy profile, which is the major concern here, is not sensitively dependent on the EOS. The entropy gradient is proportional to the difference between actual and adiabatic temperature gradient which in MLT is related to the convective flux. Hence, the constraint that a nominal total flux has to be transported essentially fixes the entropy gradient irrespective of the EOS employed, while the temperature profile is noticeably affected by the choice of the EOS.

Following the conventional way to treat the atmosphere in stellar structure models we prescribe a certain $T(\tau)$ -relation representing the temperature run in the optically thin regions. Its significance for the envelope structure emerges from the fact that it determines the level of the entropy minimum in the deeper atmosphere where the stratification becomes convectively unstable (the starting level for the entropy jump). In evolutionary calculations various descriptions of the atmosphere are commonly used, differing in the level of sophistication between simple analytical or empirical $T(\tau)$ -relations and full-fledged model atmospheres. Here we chose a $T(\tau)$ -relation that mimics closely the average atmospheric structure of the hydrodynamical models. We reproduce in particular the atmospheric entropy minimum found in the hydrodynamical models. The hydrodynamical models predict an average temperature structure in the deeper photosphere (around $-2 < \log \tau_{\text{ross}} < 0$) that closely resembles a stratification in radiative equilibrium. We emphasize that this statement refers to an averaging of the temperature on surfaces of constant optical depth in the RHD models. This averaging procedure preserves the radiative flux properties of the RHD models to a good approximation (see Steffen et al. 1995), and hence appears suitable to characterize their atmospheric structure in the present context since radiative surface cooling plays the dominant role for the convection driving.

In practice, we used an analytical fit to the exact grey $T(\tau)$ -relation for an atmosphere in radiative equilibrium according to Unsöld (1955) in envelope models intended for comparison with RHD models adopting grey radiative transfer. From the small set of RHD models adopting frequency-dependent radiative transfer we derived the average $T(\tau)$ -relation and constructed an analytical fit to it. Later in this paper we shall discuss the role of grey versus frequency-dependent radiative transport in the RHD models, demonstrating the need for a clean distinction between both types of $T(\tau)$ -relations.

The influence of the $T(\tau)$ -relation grows as the entropy jump itself decreases, so it is largest for models at low effective temperature and high gravitational acceleration. In earlier papers on the subject (Ludwig et al. 1996, 1997) we used

$T(\tau)$ -relations which were not selected on a strictly differential basis, leading to systematic differences between the older and the present calibration of α_{MLT} . Figure 2 illustrates the match of the atmospheric entropy minima. (The range in optical depth over which the RHD models are plotted do not represent the full extension of the RHD models.) Our present procedure gives now an improved match with the largest deviation found for the (4500, 4.44) model. We expect that a further improved fit of the atmospheric stratification of the RHD model would lead to an increase of α_{MLT} . But note that using the α_{MLT} derived from models in this region of the HRD would produce a consistent s_{env} in a stellar structure model as long as it is basing on a description of the stellar atmosphere by a $T(\tau)$ -relation resembling an atmosphere in radiative equilibrium.

As a side-issue the Fig. 2 demonstrates that in RHD models the higher atmospheric layers are systematically cooler than in an atmosphere in radiative equilibrium. This is due to the situation that in a convective atmosphere the temperature is governed by the competition between adiabatic cooling of overshooting material and heating by the radiation field. Quantitatively, our grey RHD models overestimate the temperature reduction since they do not include the important heating by spectral lines in the higher layers. However, as we will see in the next section this is of minor importance for the determination of α_{MLT} . The deviations between average RHD stratification and envelope models underline that our calibrated α_{MLT} only fits the asymptotic entropy and the entropy jump. The overall stratification is not well matched by an envelope model with the fitted α_{MLT} .

Effects of *turbulent pressure* are ignored in the envelope models. This is not only done for computational convenience but also reflects our opinion that the recipes provided for its treatment in the framework of MLT overestimate the effects, doing more harm than good when included. In MLT the convective motions are restricted to the unstable layers according to the Schwarzschild criterion. At the upper boundary of a surface convective zone this produces a sharp decline of the convective velocity amplitude and a correspondingly large gradient of the turbulent pressure that alters the hydrostatic structure of a model significantly. In contrast, hydrodynamical models (see Freytag et al. 1996) predict a rather smooth run of the velocity amplitude in that region with a correspondingly smaller gradient of the turbulent pressure. Clearly, the inclusion of turbulent pressure in 1D envelope models requires a proper treatment of overshooting.

Finally, it is important to realize that a unique formulation of MLT does not exist. Rather, *different versions of MLT* are in use. In the following we refer to the version of MLT originally given by Böhm-Vitense (1958). To further elaborate this point, we explicitly present details of our MLT implementation together with commonly used other formulations in Appendix A.

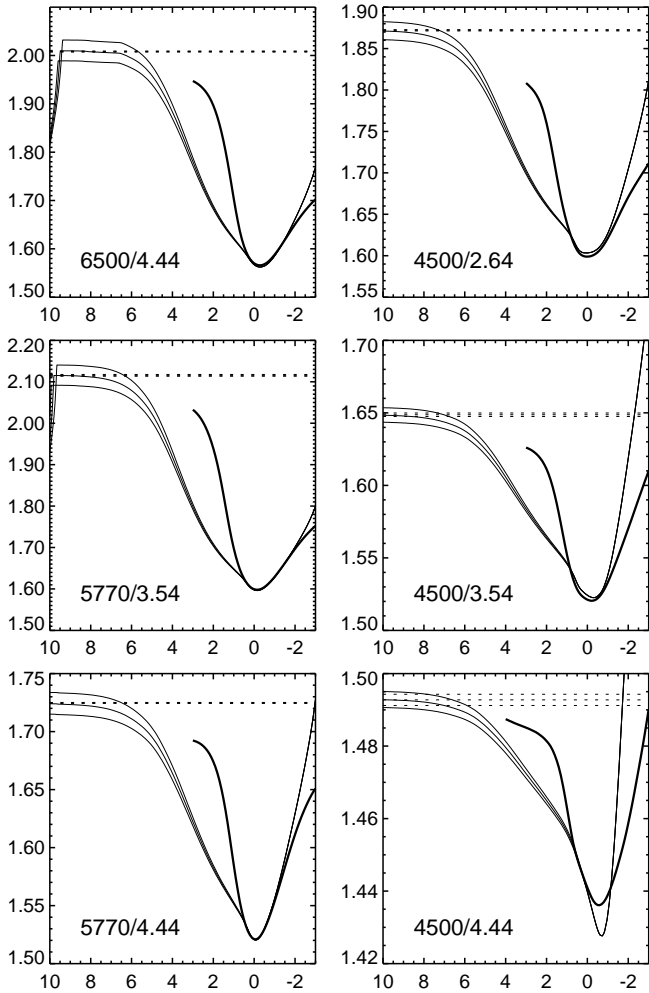


Fig. 2. Representative examples of entropy profiles (in units of $s_0 = 10^9$ erg/g/K) as a function of Rosseland optical depth $\log \tau_{\text{Toss}}$. Each panel shows the τ -averaged entropy of a RHD model (thick solid line) with envelope models (thin solid lines) for the matching α_{MLT} and $\alpha_{\text{MLT}} \pm 0.05$ for a given $T_{\text{eff}}/\log g$ combination. In all models the radiative transfer was treated in the grey approximation. The dotted horizontal lines indicate s^* of the RHD model and its temporal RMS-fluctuations. Note the significantly different entropy jumps.

3. The solar benchmark

The natural benchmark for the scenario described above is of course the Sun. Not only are its global stellar parameters known with exceptional accuracy, but helioseismology has provided us with detailed information about the structure of the solar interior. Recent astrophysical convection theories were developed in the context of stellar evolution and tests of these theories were devised within that framework, in particular by studying their effects on the evolution of the Sun (Lydon et al. 1992, 1993a; Canuto & Mazzitelli 1991, 1992; Canuto et al. 1996). In our opinion, a more direct way for a validation of such theories is to look at the present solar structure without taking recourse to evolutionary calculations. This avoids the possibility

Table 1. Results from hydrodynamical (RHD) models and helioseismology for different helium abundances. Y : helium abundance, s_{env} : entropy in the adiabatically stratified layers in units of $s_0 = 10^9$ erg/g/K, N_ν : number of frequency bands for modeling the radiative transfer, α_{MLT} : mixing-length parameter. The data for $Y = 0.246$ are obtained by linear interpolation between the data for $Y = 0.24$ and 0.28 .

Source	Y	N_ν	s_{env}/s_0	α_{MLT}
RHD	0.28	1	1.723	1.577
RHD	0.28	5	1.738	1.588
RHD	0.24	1	1.782	1.609
RHD (<i>inferred</i>)	0.24	5	1.800	1.609
Helioseismology	0.24	-	1.778	1.727
Helioseismology	0.28	-	1.736	1.594
RHD	0.246	5	1.791 ± 0.01	1.61 ∓ 0.05
Helioseismology	0.246	-	1.771 ± 0.005	1.71 ∓ 0.02

that evolutionary changes of the solar structure interfere with model properties that are used for the assessment of the accuracy of the convection theory under consideration.

In the following we shall compare our RHD model predictions for s_{env} with related helioseismic measurements. On an absolute scale any deviation from the actual physical situation, e.g. in composition, shows up as mismatch between observations and theoretical predictions without being necessarily related to flaws in the convection model. In our solar models we paid particular attention to the role of the *helium content* Y and *details of the radiative transfer*.

Table 1 summarizes the findings for the Sun. For interpreting the different entropies given in the table we note here that the entropy jump over the superadiabatic layers in the Sun amounts to $\approx 0.2 s_0$. The first block of data (4 entries) in Table 1 refers to RHD models. For solar effective temperature and gravitational acceleration we calculated RHD models with $Y = 0.24$ in addition to models with our standard $Y = 0.28$. We considered RHD models where the radiative transfer was treated in grey approximation ($N_\nu = 1$), and where its frequency dependence was approximately taken into account using 5 representative frequency bands ($N_\nu = 5$, for details about the radiative transfer scheme see Ludwig et al. 1994). The entropies s_{env} of the adiabatic part of the convective envelopes are based on the assumption $s_{\text{env}} = s^*$. The entropies derived from the RHD simulations were converted into an effective mixing-length parameter α_{MLT} as outlined above.

There is a noticeable dependence of s_{env} on the treatment of the radiative transfer and the helium content. The different treatment of the radiative transfer leads to a different atmospheric temperature structure, resulting in a change of the absolute entropy level in the deeper atmosphere. There is some further influence on the entropy jump itself since the radiative energy exchange in the surface layers is slightly modified. But

despite significant differences in s_{env} for the two RHD models with $Y = 0.28$, both models give the same α_{MLT} values within the uncertainty of α_{MLT} of ± 0.05 . This is achieved by comparing RHD models and envelope models on a strictly differential basis. The $T(\tau)$ -relation in the envelope models was selected to closely follow the relation found in the RHD models: RHD models basing on grey radiative transfer were compared to envelope models calculated with a grey $T(\tau)$ -relation in their atmospheric layers. For RHD models basing on frequency-dependent radiative transfer, a $T(\tau)$ -relation was derived by horizontally and temporally averaging their temperature structure on surfaces of constant optical depth. This $T(\tau)$ -relation was subsequently used in the calculation of the related envelope models. When mixing solar RHD and envelope models with incompatible $T(\tau)$ -relations, α_{MLT} changes by up to 0.1. We have performed the same tests for a hotter RHD ($T_{\text{eff}} = 6500 \text{ K}$) model with similar findings. The insensitivity of α_{MLT} with respect to the treatment of the radiative transfer allowed us to largely rely on computationally less demanding RHD models employing grey radiative transfer for studying the scaling of α_{MLT} across the HRD.

The entropy difference due to a change in the helium content is primarily related to the associated change of the mean molecular weight. To first order, the RHD models react to changes in Y by keeping the temperature-pressure structure invariant. The density scales in proportion to the change in molecular weight (here: $\mu(Y = 0.28)/\mu(Y = 0.24) = 1.037$); entropy and internal energy per unit volume remain the same, allowing the model to transport the same energy flux without a change of the flow velocity. The simple scaling behaviour of the RHD models with Y and the invariance of α_{MLT} found in the case $Y = 0.28$ lead us to derive the values for $Y = 0.24$, $N_{\nu} = 5$ from an envelope model *assuming* the same α_{MLT} as in the case $Y = 0.24$, $N_{\nu} = 1$. The entry for this model in the table is flagged as “inferred”.

The second block of data (2 entries) in Table 1 shows results derived from helioseismic considerations. Helioseismology provides the sound speed-density profile in the Sun with high accuracy. In the deeper, adiabatically stratified layers of the envelope this profile defines an adiabat in the sound speed-density plane. If chemical composition and the EOS are known one can label this adiabat with its actual entropy value. Note that only thermodynamic properties enter into this procedure; it is independent of opacity or results from stellar structure models as long as one regards the helioseismic measurements themselves as independent. The helioseismic entropy values of the second block of data in Table 1 are derived in this way by assuming a certain Y and adopting the OPAL EOS (Rogers et al. 1996) to establish the relation between sound speed, density, and entropy. The α_{MLT} values are again derived from envelope models that match s_{env} . In contrast to s_{env} , the determination of α_{MLT} depends on low-temperature opacities and stellar structure considerations. The helioseismic data are due to Antia (1996) and were kindly made available to us by the author.

The third block of data (2 entries) finally summarizes our best estimates for s_{env} from RHD models and helioseismology.

They were obtained by linear interpolation between the data for $Y = 0.24$ and $Y = 0.28$ to Antia’s (1996) best helioseismic estimate for the helium content $Y = 0.246$ based on the OPAL EOS. The uncertainties given in the helioseismic case are dominated by the uncertainty of the helium content. We have adopted an uncertainty of ± 0.005 , roughly comprising the range of Y discussed in the literature. In the RHD case the uncertainties reflect the variations which we find between simulation runs for the same physical parameters that differ in numerical details (grid resolution, size of the computational box, explicit or implicit treatment of the energy equation, etc.).

Of course, all our error estimates do not include possible systematic effects. The helioseismic Y can be affected by systematic errors in the EOS. The RHD results are certainly affected by the two-dimensionality of the models. Indeed, we interpret the discrepancy between RHD and helioseismic results as systematic effect: our 2D RHD models overestimate s_{env} by $0.02 s_0$ (10% of the overall entropy jump between the surface and the adiabatic layers) and correspondingly underestimate the solar α_{MLT} by 0.1. This conclusion is supported by first results from a differential comparison of 2D and 3D RHD simulations for the Sun. The 3D run predicts a smaller s_{env} by $0.013 s_0$, corresponding to a larger α_{MLT} by 0.07. Taking this fact into consideration, the theoretical and observational determination of α_{MLT} become fully consistent.

We expect another systematic effect to influence the absolute value of α_{MLT} affecting both the observationally and the theoretically derived values in the same manner. There exist indications that our low-temperature opacities underestimate the real stellar opacity in the deeper, subphotospheric layers. Our differential approach for determining α_{MLT} cannot fully compensate for this deficiency since the opacities affect RHD and MLT models differently. In RHD models the opacity effects are confined to the very thin cooling layer on top of upflowing regions, while in MLT models the opacities are important all over the zone of high superadiabaticity. This biases our α_{MLT} values again towards lower values. In the region of high superadiabaticity our opacities are presumably too small by 10–20%, causing α_{MLT} to be underestimated by ≈ 0.1 .

However, in view of the fact that the RHD models are essentially parameter-free we consider the match in 2D as satisfactory. Besides the zero point, the functional dependence of s_{env} and α_{MLT} on the fundamental stellar parameters is of major interest. We believe that for these scaling relations our error estimates based on purely intrinsic model uncertainties are well justified.

4. Calibration data for solar-type stars

As for the Sun, we studied the behaviour of s_{env} and α_{MLT} over the HRD in the solar neighbourhood. This investigation demanded a large number of simulation runs since we had to cover many objects and had to clarify how densely the HRD should be sampled in order to record the relevant variations of α_{MLT} . The results are now based on 58 simulation runs for solar metallicity and $Y = 0.28$, covering the range $4300 \text{ K} \leq$

$T_{\text{eff}} \leq 7100 \text{ K}$ and $2.54 \leq \log g \leq 4.74$. Corresponding results for metallicities down to $[M/H] = -2$ will be published in a subsequent paper.

Various aspects determined the region of the HRD which is covered by our models: Towards higher T_{eff} the convective zones become shallow and hence insignificant for the overall stellar structure. Towards lower T_{eff} molecular opacities become more and more important; these are not included in our opacities yet. Moreover, convection becomes very efficient, leading to small entropy jumps which cause problems in the numerical modeling. Towards lower $\log g$ the large entropy jumps cause other numerical problems related to the steep temperature and velocity gradients in the surface cooling layer. And finally, no solar-type stars are located towards higher $\log g$.

We present our findings in graphical as well as numerical form. Like in the solar case, several RHD simulation runs differing in numerical details were performed for certain atmospheric parameter combinations, thus allowing us to estimate the internal uncertainties associated with our models. In the figures we provide numerical values and show polynomial or exponential least-squares fits to the data points. The fits are constructed such that the residuals between fitted and actual data values show no remaining systematic dependence on the stellar parameters. In Appendix C we give explicit expressions for these fits. In this way our results can be easily utilized in other applications. We made efforts to produce fits with a simple and smooth functional dependence. Nevertheless we remind the reader to the fact that polynomial fits of higher order are not well suited for extrapolation. In other words: the fits quickly lose their meaning outside the region covered by the grid of RHD models and should not be extrapolated too far!

Figure 3 displays s_{env} as a function of T_{eff} and $\log g$ in the HRD. In the region where $s_{\text{env}} > 2.6 \times 10^9 \text{ erg/g/K}$, convection becomes inefficient and the convective zones are superadiabatic throughout. Entropies in that region refer to the value encountered at the base of the convective envelope and are still derived assuming $s_{\text{env}} = s^*$. Besides s_{env} itself, the entropy jumps are of interest since they measure the efficiency of the convective energy transport. The entropy jumps shown in Fig. 4 are the entropy differences between the photospheric entropy minimum on the optical depth scale and s_{env} (see Fig. 2).

Figure 4 shows that the RHD model grid covers more than an order of magnitude in the entropy jump, comprising stars with rather efficient envelope convection (with small entropy jumps) in the regions of K-dwarfs and stars with inefficient convection (large entropy jumps) in the region of F-dwarfs. The significant variation of the entropy jumps indicates that the simple dependence of s_{env} seen in Fig. 3 is non-trivial. It is not just reflecting the changes of the stellar surface conditions due to changes of opacity and ionization balance but carries information about changes in the efficiency of the convective energy transport.

With the aid of envelope models (as described before) we translated the s_{env} values given in Fig. 3 into equivalent mixing-length parameters which are shown in Fig. 5. We find a moderate, nevertheless significant variation of α_{MLT} between

about 1.3 for F-dwarfs and 1.75 for K-subgiants. In the close neighborhood of the Sun we find a plateau where α_{MLT} remains almost constant. As discussed previously, the absolute values of α_{MLT} are probably less reliable than its scaling properties as displayed in Fig. 5.

The theory of Canuto & Mazzitelli (1991,1992; CMT) describes convection analytically within the picture of a turbulent medium. In view of the significant amount of work that went into the implementation and verification of this prescription by several groups, it appeared worthwhile to compare our results with CMT. Like MLT, CMT contains a free length-scale Λ . According to Canuto & Mazzitelli Λ is essentially the distance to the upper (Schwarzschild) boundary of the convective envelope; for purposes of fine tuning they add a small fraction of the pressure scale height at the upper boundary. We follow this recipe here by writing $\Lambda = z + \alpha_{\text{CMT}} H_{\text{P,top}}$ and translated our s_{env} to α_{CMT} values, again with the help of envelope models, but now based on CMT. As shown in Fig. 6, we find $\alpha_{\text{CMT}} \approx 0.4$ for the Sun. To assess the sensitivity of s_{env} to α_{CMT} , we note that the overall entropy jump at fixed solar T_{eff} and $\log g$ increases by roughly a factor of 2 if one reduces α_{CMT} from 0.4 to zero. As in the MLT case, we find a region of rather constant α_{CMT} in vicinity of the Sun and a significant variation between zero in the region of K-dwarfs and almost 0.6 for F-dwarfs. Interestingly, for the model with the lowest T_{eff} , we find an α_{CMT} slightly smaller than zero. This value was formally derived by extrapolating the $s_{\text{env}}(\alpha_{\text{CMT}})$ -relation towards negative α_{CMT} .

5. Implications and discussion

5.1. Calibrating α_{MLT} with evolutionary models of the Sun?

The RHD models predict almost no change of α_{MLT} during the solar main-sequence evolution and at most a very weak dependence of the convective efficiency on the helium abundance in the convective envelope (see Fig. 5 and Table 1). This is an important piece of information since it justifies the common practice of calibrating the solar α_{MLT} with evolutionary models. However, we think that the accurate knowledge about the solar envelope structure from helioseismology now provides a cleaner way to calibrate the efficiency of solar convection by the procedure outlined in Sect. 3. Calibrating α_{MLT} with the help of the present envelope structure would provide insight into the validity of parts of the physics put into the evolutionary model calculations.

For instance, calibrated solar models with and without element diffusion, respectively, provide different values for α_{MLT} (cf. e.g. Richard et al. 1996). Models including diffusion give a lower helium abundance at the surface for the present Sun and a somewhat higher α_{MLT} than models without diffusion. This might appear to contradict our findings, namely that α_{MLT} is almost independent of the helium content. The reason is of course that the evolutionary models without diffusion do not represent the Sun since their present surface helium abundance is not the actual one. This shortcoming of an evolutionary model without diffusion is compensated for by a change of

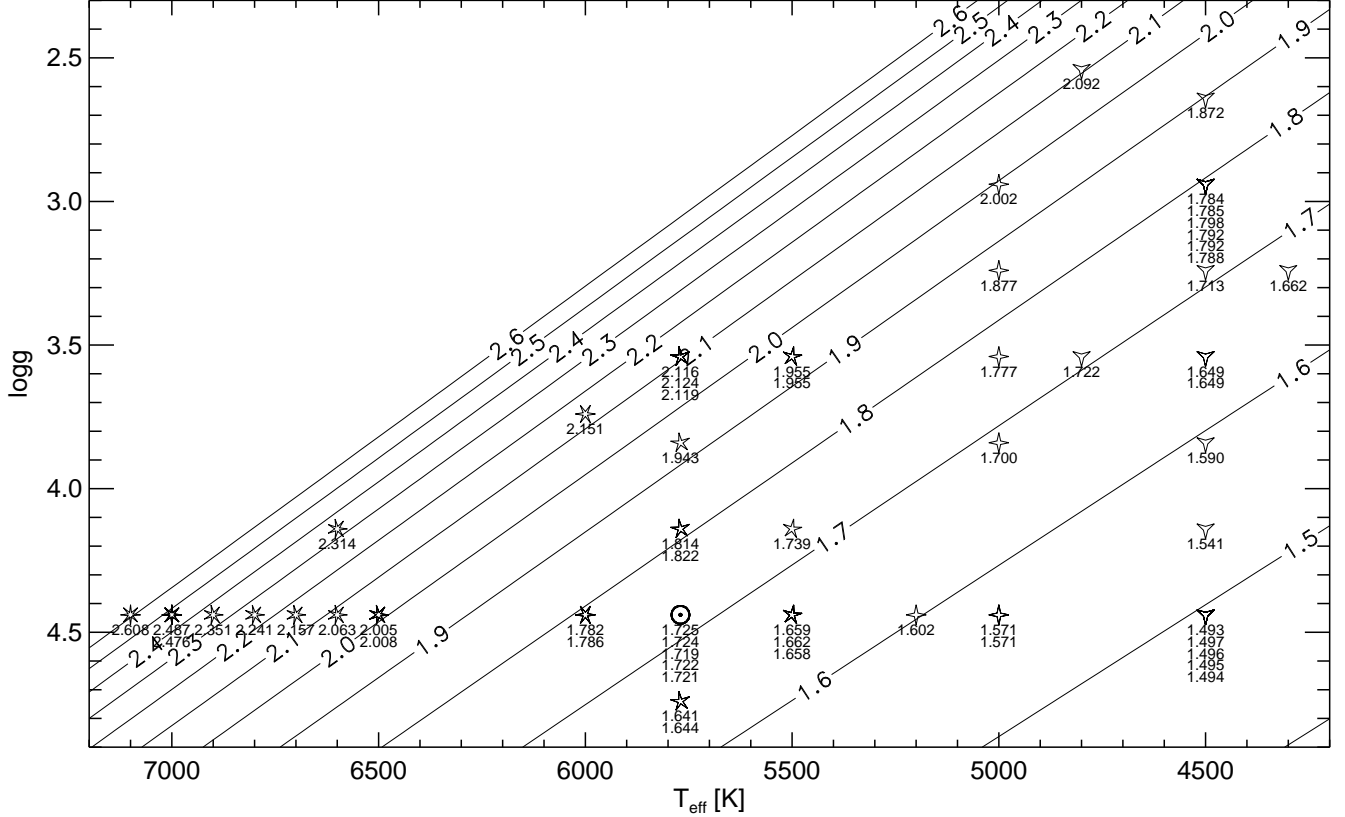


Fig. 3. s_{env} in units of $s_0 = 10^9$ erg/g/K from the grid of RHD models for $Y = 0.28$ and solar metallicity. Symbols indicate RHD models. Attached to the symbols the actual s_{env} values are given; the contour lines present a fit to them. The fitting function is given in Appendix C.

α_{MLT} . As a price, no assessment of the quality of the model or the adequacy of the input physics is possible any more. If, however, one calibrated α_{MLT} at the present envelope structure, shortcomings in the input physics would not be hidden in the α_{MLT} calibration but would show up as a mismatch between the predicted and the actual solar radius.

5.2. How to make best use of the calibration data in evolutionary models?

In the case of the Sun our calibration underestimates the absolute value of the mixing-length parameter by about $0.1 \dots 0.2$, a value which can be explained by a combined systematic effect due to the too small low-temperature opacities and the 2D approximation. The scaling behaviour of the α_{MLT} with effective temperature and surface gravity is a differential result and will be much less affected by these systematic shortcomings. From this perspective it seems that a scaling of the α_{MLT} values presented here by a constant factor (slightly larger than unity) is still admissible. In the context of stellar evolutionary models we suggest to calibrate α_{MLT} at the present Sun and use the ratio to α_{MLT} from our calibration as a scaling factor. We propose a constant scaling factor since it appears plausible to compensate for the systematic offset seen in the Sun in a simple, homogeneous fashion. For the time being this is the

best one can do since the Sun is the only star where we know α_{MLT} with sufficient accuracy to critically test our results observationally. However, we emphasize that at the moment the scaling is a well-motivated modification to our results. We expect to eliminate the necessity of this step by improving on the identified systematic shortcomings of our approach in future models.

The simplified radiative transfer in the RHD models provides only an approximate atmospheric $T(\tau)$ -relation. We have seen by comparison of grey and non-grey models that the influence of the $T(\tau)$ -relation on the determination of α_{MLT} can be strongly reduced if one sticks to the same approximation in the envelope and RHD models. In this way we separated to some extent properties of convection from issues related to opacities and radiative transfer. If one now aims at a comparison with observations, the radiative properties should be modeled as accurately as possible. In evolutionary models intended to reproduce observations (e.g. colors) one should use as accurate $T(\tau)$ -relations as possible, preferentially derived from full-fledged model atmospheres. The α_{MLT} values from our calibration are not affected by such a change to a moderately differing $T(\tau)$ -relation.

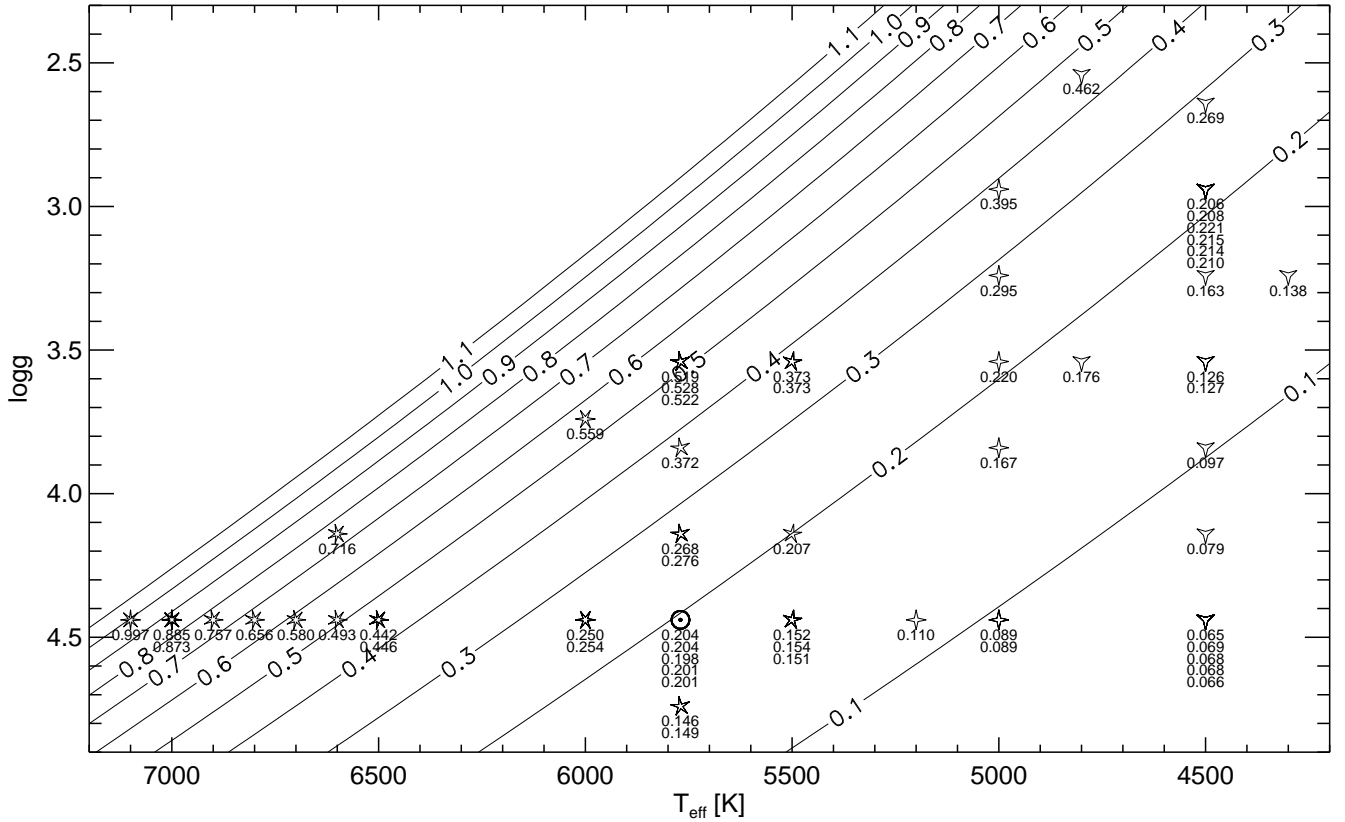


Fig. 4. Entropy jumps in units of $s_0 = 10^9$ erg/g/K. The entropy jump was calculated as difference between s_{env} and the entropy at the photospheric entropy minimum. See Fig. 3 for further explanations.

5.3. Consistency with stellar stability

A variation of α_{MLT} and corresponding variation of s_{env} with the atmospheric parameters T_{eff} and $\log g$ can lead to a secular instability of a star on the Kelvin-Helmholtz timescale of its convective envelope. In order to see this, let's consider a small perturbation of s_{env} in a star's envelope. As known from stellar structure models such a disturbance alters its radius while the luminosity remains largely unchanged. The change in radius leads to a change of the surface parameters. Following Christensen-Dalsgaard (1997, his relations (10) and (12)) one approximately finds for the differential relation between s_{env} and T_{eff} valid for stars similar to the Sun

$$\left(\frac{\partial s_{\text{env}}}{\partial T_{\text{eff}}}\right)_{L=\text{const}} \approx -5 \frac{c_p}{T_{\text{eff}}} \quad (2)$$

where c_p is the typical specific heat at constant pressure in the convective envelope.

While relation (2) describes the response of the global stellar structure on changes of s_{env} the question is whether this is compatible with the surface conditions. Since from the surface conditions s_{env} is a function of T_{eff} and $\log g$, there is the possibility of a feedback on s_{env} which can amplify or damp an perturbation of s_{env} . One would obtain an amplification if s_{env} drops more strongly with T_{eff} than given by relation (2). In case of an amplification, rapid changes of the stellar surface

parameters would occur, leading to regions in the HRD devoid of stars.

Clearly, we do not observe such “gaps” in the region of the HRD studied here, and indeed one can verify with the aid of Fig. 3 that s_{env} as controlled by the surface conditions exhibits a stabilizing behaviour since

$$\left(\frac{\partial s_{\text{env}}}{\partial T_{\text{eff}}}\right)_{L=\text{const}} > 0. \quad (3)$$

Similar relations hold for the atmospheric entropy minimum (not shown) and the entropy jump (see Fig. 4). Hence, all factors influencing s_{env} suggest that the convective instability described above will not be encountered. However, at least in principle, it cannot be excluded that under special circumstances a convectively driven runaway might occur.

5.4. The gravity-darkening¹ exponent

On the surface of a slowly rotating star the relation between local T_{eff} and gravity g can be approximated by

$$T_{\text{eff}} \propto g^\beta. \quad (4)$$

¹ Sometimes also referred to as gravity-brightening!

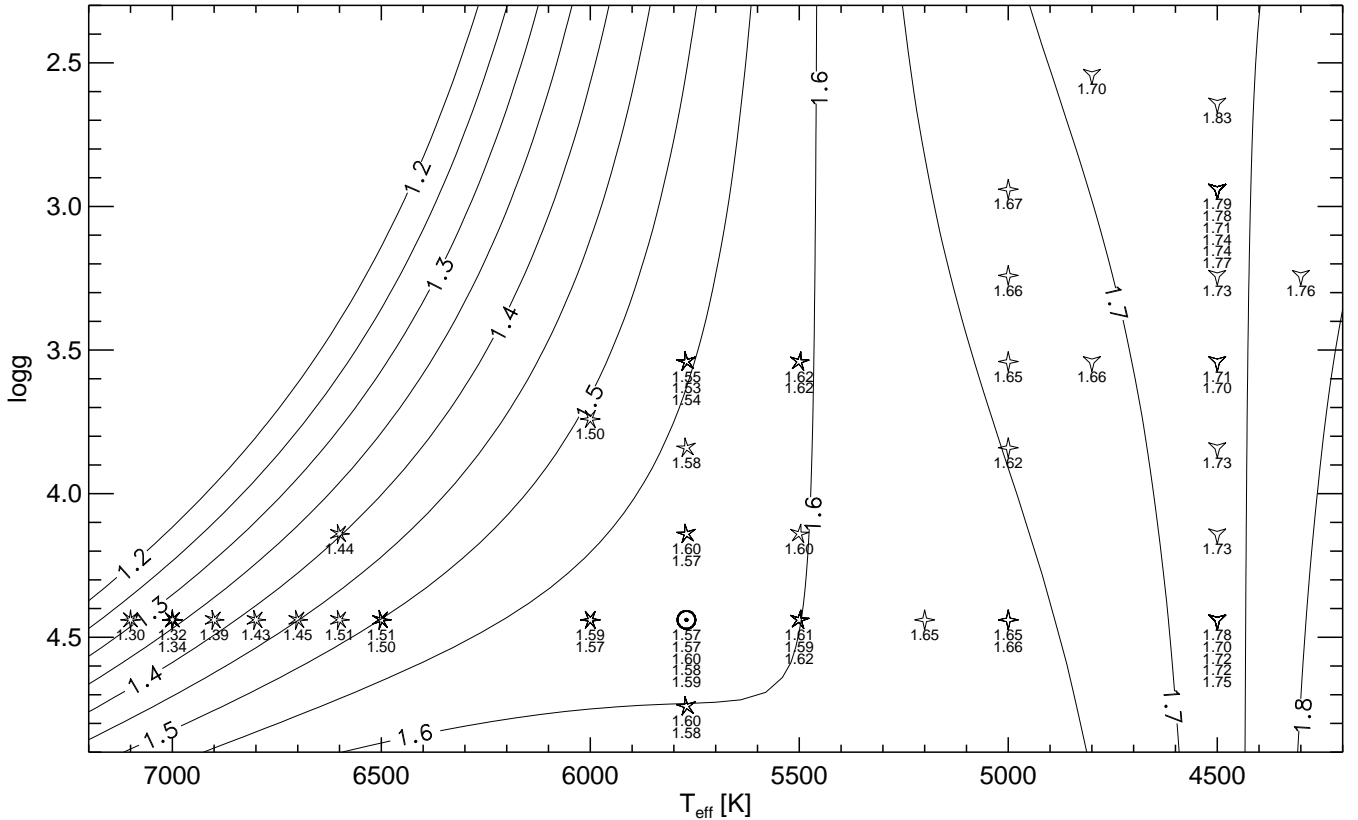


Fig. 5. α_{MLT} for standard mixing-length theory (Böhm-Vitense 1958) with $\Lambda = \alpha_{\text{MLT}} H_P$ (Λ : mixing-length, H_P : local pressure scale height). The presentation of the data is analogous to Fig. 3.

Lucy (1967) argued that the so called gravity-darkening exponent β for stars with convective envelopes is given by

$$\beta = \left(\frac{\partial \log T_{\text{eff}}}{\partial \log g} \right)_{s_{\text{env}}=\text{const}}. \quad (5)$$

Figure 3 represents lines $s_{\text{env}} = \text{const}$, so the gravity-darkening exponent given by our RHD simulations can be readily deduced from this plot. We find an increase of β from 0.07 to 0.10 when going from the F- to the K-dwarfs, and a slight decrease of β with decreasing gravity. Basically, this confirms Lucy’s result $\beta = 0.08$, with the novelty that our approach eliminates the weakest point of his analysis, namely that MLT provides a reasonable scaling relation $s_{\text{env}}(T_{\text{eff}}, \log g)$ with constant α_{MLT} . Current observations of β (see e.g. Alencar & Vaz 1997) are consistent with our findings, but show a rather large scatter and do not allow a critical test of our results. We therefore refrain from a further discussion here.

5.5. Contrasting ours with other approaches

The long-standing lack of a reliable theory of convection has prompted numerous attempts to remedy the situation. In the following we comment on the work of two groups and highlight the major differences in the involved physics between their’s and our approach, hoping to clarify the possible reasons for deviating results.

In a series of three papers Lydon et al. (1992, 1993a,b; hereafter LFS) presented a formulation of convective transport based on results of numerical experiments by Chan & Sofia (1989). The idealized numerical experiments were set up to describe the generic properties of almost adiabatic convection; radiative energy transport was included only as a diffusive flux computed with constant conductivity. Chan & Sofia extracted *local* statistical relations from their numerical data which were subsequently used by LFS to derive an expression for the convective energy flux suitable for calculating stellar structure models. LFS modeled the Sun as well as the A- and B-component of the α Centauri system. They found essentially the same α_{MLT} in all cases when they translated their formulation into an effective mixing-length parameter. This is consistent with our results, but in our opinion not a strong statement since the rather small differences in the surface parameters and chemical composition among the three stars makes it difficult to detect changes of α_{MLT} . Moreover, there is a principle problem with the LFS convection formulation since it relies on numerical experiments for adiabatic convection. In a follow-up project to the work of Chan & Sofia, Kim et al. (1995) found significantly different statistical relations among the fluctuating quantities in the superadiabatic regime, probably implying that larger uncertainties have to be attributed to the original results of LFS.

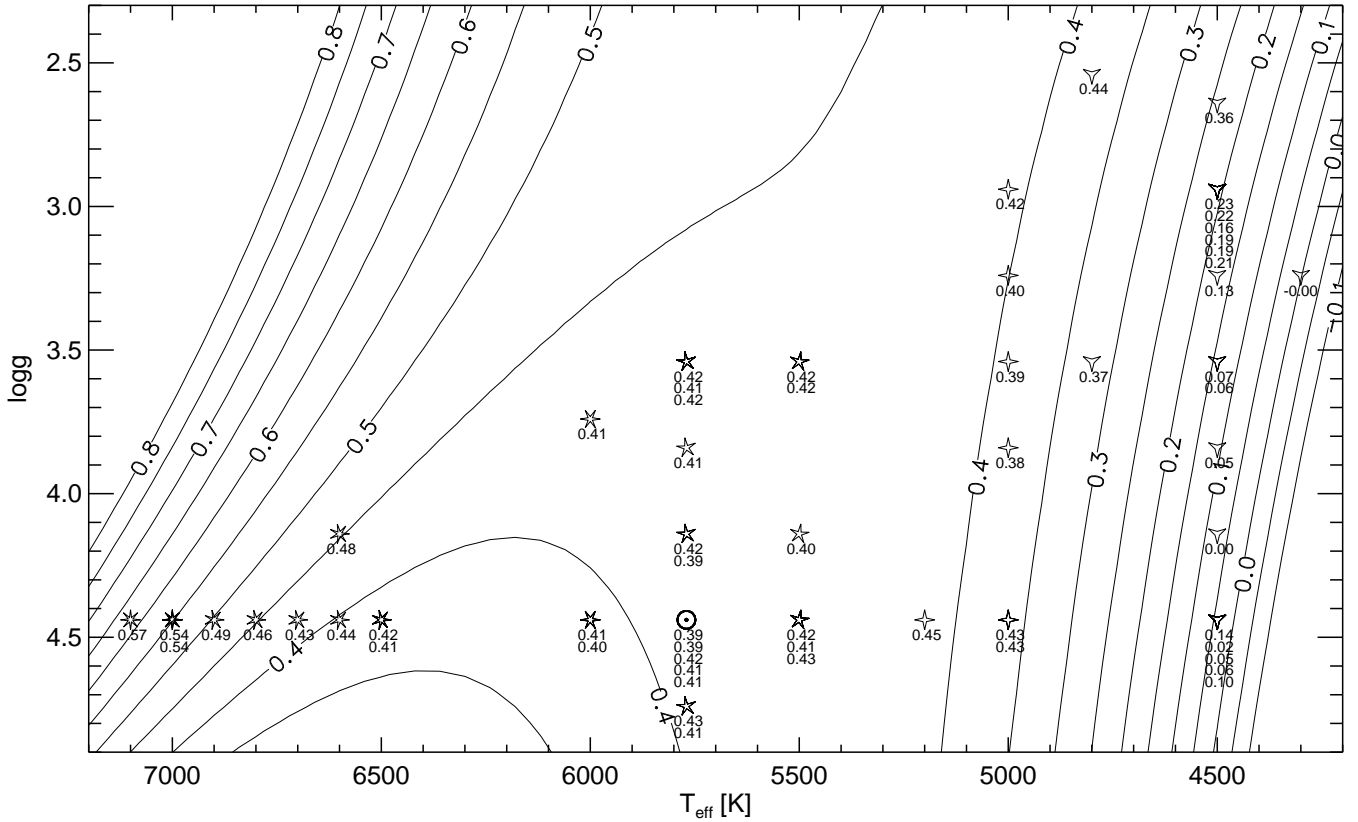


Fig. 6. α_{CMT} for the Canuto & Mazzitelli convection theory with $\Lambda = z + \alpha_{\text{CMT}} H_{\text{P,top}}$ (z : distance to the upper (Schwarzschild) boundary of the convective zone, $H_{\text{P,top}}$: pressure scale height at the upper boundary). The α_{CMT} -calibration reproduces the same underlying s_{env} -distribution as the α_{MLT} -calibration shown in Fig. 5. The presentation of the data is analogous to Fig. 3.

In CMT the main improvement with respect to MLT was the inclusion of a larger spectrum of eddies supposed to exist in a turbulent medium. Radiation was only included in a MLT-like fashion, and effects due to the compressibility of the medium were neglected. In our investigation we have regarded the characteristic length scale in CMT as a free parameter, adjusting it to fit the results of our simulations. If we compare the calibration of CMT shown in Fig. 6 with standard MLT shown in Fig. 5, we find a more extended plateau in the solar vicinity. The general tendency of CMT to make efficient convection more efficient and inefficient convection less efficient results in a smoother behaviour relative to MLT. But towards high and low effective temperatures, a clear over-compensation occurs, leading to a change of α_{CMT} . In MLT as well as in CMT, a significant variation of the free parameter is needed, and no simple scaling is apparent. We do not find a qualitative difference in their ability to reproduce s_{env} from the RHD simulations.

LFS as well as CMT essentially relate the convective flux to the *local* conditions in the flow. Such an approach is not well motivated from the simulation results where convection appears to be an extremely non-local phenomenon governed by the processes taking place in the thin cooling layer at the stellar surface (see Spruit 1997 for a recent discussion) while the bulk of the convection zone adapts to these layers. Even though we fit our simulation results to local theories, we do not assume

that convection can be described in local terms since the fit is of purely formal nature. Furthermore, both LFS and CMT treat the effects of radiative transfer in a rudimentary fashion, despite the well-known fact that for a *quantitative* description of stellar convection a proper treatment of the radiative transfer is crucial. Indeed, much effort goes into the realistic modeling of radiative transfer in our RHD simulations. CMT describes convection within the picture of incompressible turbulence. However, it is just the compressibility of the stellar gas that gives turbulence in stars its special inhomogeneous character (see Nordlund et al. 1997 for a detailed discussion). In contrast, our RHD simulations fully include the effects of compressibility.

6. Concluding remarks

We presented a calibration of the asymptotic entropy s_{env} and the corresponding mixing-length parameter α_{MLT} for solar-type stars basing on radiation-hydrodynamics models. Despite the fact that s_{env} is all that is needed to construct a stellar structure model, it was helpful to translate s_{env} into a corresponding α_{MLT} since α_{MLT} proved to be less sensitive to the physical and numerical input to the models than s_{env} itself. We gave only a description of the numerical results without providing an explanation in physical terms — not even on a qualitative level — of the scaling behaviour of α_{MLT} which we observe.

We shall come back to this interesting issue in the next paper of this series where we can look at it from a broader perspective by including models of sub-solar metallicity.

Figure 3 shows a remarkably simple structure if one considers the complex interplay of fluid flow and radiation which governs the dependence of s_{env} on the stellar parameters. Certainly, the simplicity of this dependence is a major reason for the relative success of MLT to predict s_{env} , as evidenced by the moderate variation of α_{MLT} in Fig. 5. Looking at relative changes ignores the more fundamental problem of fixing the absolute value of α_{MLT} , which in practice is done by taking recourse to empirical constraints. Our RHD models provide a determination of the zero point from first principles. Since in MLT important pieces of the physics of convection are missing — at least within the present physical interpretation of the MLT formulae — our work should not be considered as validation of MLT, even though MLT is capable of matching some of our simulation results quite well.

Work is under way to check and apply the hydrodynamical convection models beyond the comparison with the Sun. There are classical procedures which allow the determination of the convective efficiency at various locations in the HRD (position of the red giant branch, shape of the main sequence, evolution of binary stars). A lot of work has already been dedicated to empirical determinations, but conclusions are sometimes conflicting and no clear picture has emerged yet. We suspect that systematic uncertainties are actually often larger than estimated. E.g. Castellani et al. (1999) emphasize discrepancies in fitting the main sequence of open clusters which are related to the temperature-color transformation and the uncertainties in α_{MLT} . Clearly, with an independent calibration of α_{MLT} at hand one can disentangle both effects. For the case of globular clusters Freytag & Salaris (1999) have studied the effects which are expected from our calibration on the shape of the turn-off and the position of the red giant branch. By using our calibration the effective temperatures of their evolutionary models become essentially unaffected by the uncertainties inherent to MLT. The uncertainties related to the temperature-color transformation remain present but one can at least judge the internal accuracy of the transformation. The precise HIP-PARCOs data — in particular for some open clusters — might allow a detailed investigation of these issues. Moreover, helioseismology proved to be an invaluable tool in the case of the Sun, and asteroseismic measurements of the internal stellar structure appear to be a promising way to gain further insight.

Already in 2D, the construction of *hydrodynamical model grids* is computationally demanding. Nevertheless, the step towards 3D models is desirable, and first calibrations of α_{MLT} from 3D models are now available for smaller stellar samples: Trampedach et al. (1997) presented a calibration based on 6 models in the solar vicinity, Abbott et al. (1997) presented a calibration for the Sun. The latest version of the calibration of Trampedach et al. (Trampedach 1998, priv. comm.) is consistent with our calibration except for a systematic offset which is caused by differences in the employed low-temperature opacities; the scaling behaviour is similar as far as it is possible to

judge from the small set of models. Abbott et al. do not provide α_{MLT} with sufficient precision to allow a critical comparison with our results. Own work is in progress to quantify systematic differences between 2D and 3D models. As already mentioned, first results for the Sun give a change of α_{MLT} by +0.07 with respect to the 2D models. We expect systematic changes of similar magnitude for other stars. Hence, it appears unlikely that conclusions of this paper will have to be altered substantially when more 3D results become available.

Last but not least we want to reiterate the warning that the presented calibration of α_{MLT} is only intended to reproduce s_{env} and the entropy jump. The detailed temperature profile of the superadiabatic layers is not necessarily represented adequately by an MLT model with our calibrated α_{MLT} (see Fig. 2). Moreover, the calibration is not suitable for providing the optimum mixing-length parameter for convective stellar atmospheres. Preliminary results for the Sun (Steffen & Ludwig 1999) show that matching the *emergent radiation field* of multidimensional simulations with 1D standard atmospheric models requires a quite different mixing-length parameter than is needed for matching the entropy jump. We do not consider this as a contradiction; it just indicates shortcomings of MLT and the 1D idealization.

Acknowledgements. During the course of the project, many colleagues helped with discussions, opinions, and criticism. HGL is particularly grateful to Norbert Langer, Hendrik Spruit, Maurizio Salaris, Scilla Degl'Innocenti, Achim Weiss, Philipp Podsiadlowski, Hans Ritter, and Regner Trampedach. BF acknowledges financial support by the Deutsche Forschungsgemeinschaft under grant Holweger 596/36-1. MS expresses his thanks to the University of Kiel for its kind hospitality and for providing access to its computing facilities.

Appendix A: Mixing-length formulations

Generically, the well-known equations of MLT (cf. Cox & Giuli 1968) for the convective efficiency

$$\Gamma \equiv \frac{\nabla - \nabla_e}{\nabla_e - \nabla_{\text{ad}}} = \frac{\rho c_p v_c \tau_e}{f_3 \sigma T^3} \left(1 + \frac{f_4}{\tau_e^2} \right), \quad (\text{A.1})$$

the convective velocity

$$v_c^2 = f_1 \frac{\Lambda^2 g \delta (\nabla - \nabla_e)}{H_P}, \quad (\text{A.2})$$

and the convective flux

$$F_c = f_2 \frac{\rho c_p v_c T \Lambda (\nabla - \nabla_e)}{H_P} \quad (\text{A.3})$$

contain four dimensionless free parameters f_1 , f_2 , f_3 , and f_4 . In the equations, the optical thickness of a convective eddy τ_e and the isobaric expansion coefficient δ are defined as

$$\tau_e \equiv \chi \rho \Lambda, \quad \delta \equiv - \left(\frac{\partial \ln \rho}{\partial \ln T} \right)_P. \quad (\text{A.4})$$

Further quantities entering the equations are the mixing-length Λ , specific heat at constant pressure c_p , Stefan-Boltzmann's constant σ , density ρ , temperature T , actual

Table A.1. Constants f_i for the MLT formulations of various authors. (ML1 and ML2 are commonly used terms in the white dwarf community.)

Formulation	f_1	f_2	f_3	f_4
Böhm-Vitense 1958, ML1	$\frac{1}{8}$	$\frac{1}{2}$	24	0
ML2	1	2	16	0
Mihalas 1978, Kurucz 1979	$\frac{1}{8}$	$\frac{1}{2}$	16	2
Heney et al. 1965	$\frac{1}{8}$	$\frac{1}{2}$	$\frac{4\pi^2}{24}$	$\frac{4\pi^2}{3}$

temperature gradient ∇ , temperature gradient of a convective eddy ∇_e , and adiabatic gradient ∇_{ad} (∇ stands for $\partial \ln T / \partial \ln P$). Table A1 provides the f -parameters for various MLT formulations. The values of α_{MLT} given in this paper refer to the MLT formulation by Böhm-Vitense (1958) as specified in the first row of the table.

A fine point in our implementation of MLT concerns the evaluation of the radiative gradient ∇_{rad} . We do not use the commonly adopted expression for the radiative gradient in diffusion approximation, but instead derive ∇_{rad} by differentiation of the $T(\tau)$ -relation. As a starting point, consider the $T(\tau)$ -relation for a grey atmosphere in radiative equilibrium

$$T^4 = \frac{3}{4} T_{\text{eff}}^4 [\tau + q(\tau)]. \quad (\text{A.5})$$

While in the case of a grey atmosphere q is the Hopf-function, we can introduce a modified q such that Eq. A.5 represents any prescribed $T(\tau)$ -relation. A reasonable q should have the property

$$\lim_{\tau \rightarrow \infty} q = \text{const} \quad (\text{A.6})$$

which guarantees that ∇_{rad} becomes independent of τ and consistent with the diffusion approximation for large optical depth (provided the Rosseland scale is adopted). The advantage of this procedure is that we obtain a smooth and realistic ∇_{rad} which is consistent with the specified $T(\tau)$ -relation irrespective of optical depth. We never have to distinguish between atmosphere and optically thick layers and can use MLT throughout, for the small price of having to compute the τ -scale as well.

Appendix B: Entropy scale

The entropy is not always available from an EOS, and if so it involves an arbitrary additive constant. In order to relate entropy values given in this paper to more common thermodynamic variables, we provide a small list of quantities as a function of entropy and pressure in Table B1, calculated from the EOS which was used in the RHD simulations. We have concentrated on higher temperatures characteristic of the deeper layers of solar-type stellar envelopes. The data should allow to interrelate values for s_{env} to pressures, temperatures, and densities, and provide the entropy zero point of our EOS. For in-

Table B.1. Thermodynamic quantities as a function of entropy and pressure from the RHD EOS for solar metallicity and $Y = 0.28$. Unless noted otherwise the values are given in cgs-units.

s/s_0	$\log P$	$\log T$	$\log \rho$	Γ_1	δ	$c_p/10^8$
1.50	8.0	4.310	-4.218	1.277	1.980	10.146
1.50	9.0	4.487	-3.457	1.355	1.915	9.000
1.50	10.0	4.715	-2.746	1.467	1.616	6.608
1.50	11.0	5.022	-2.096	1.591	1.276	4.435
1.50	12.0	5.375	-1.473	1.631	1.182	4.006
1.50	13.0	5.759	-0.868	1.663	1.104	3.602
1.75	8.0	4.406	-4.415	1.316	1.948	11.121
1.75	9.0	4.618	-3.684	1.436	1.468	6.733
1.75	10.0	4.933	-3.032	1.577	1.124	4.074
1.75	11.0	5.283	-2.401	1.634	1.072	3.727
1.75	12.0	5.675	-1.797	1.665	1.023	3.406
1.75	13.0	6.074	-1.197	1.667	1.015	3.373
2.00	8.0	4.531	-4.616	1.415	1.320	6.370
2.00	9.0	4.859	-3.966	1.534	1.081	4.169
2.00	10.0	5.201	-3.325	1.646	1.026	3.520
2.00	11.0	5.598	-2.723	1.666	1.004	3.352
2.00	12.0	5.998	-2.123	1.667	1.003	3.344
2.00	13.0	6.398	-1.523	1.667	1.002	3.342
2.25	8.0	4.789	-4.899	1.474	1.090	4.641
2.25	9.0	5.124	-4.249	1.655	1.010	3.419
2.25	10.0	5.523	-3.648	1.667	1.001	3.341
2.25	11.0	5.923	-3.048	1.667	1.000	3.339
2.25	12.0	6.323	-2.448	1.667	1.000	3.338
2.25	13.0	6.723	-1.848	1.667	1.000	3.338
2.50	8.0	5.049	-5.174	1.660	1.004	3.377
2.50	9.0	5.448	-4.574	1.667	1.000	3.338
2.50	10.0	5.848	-3.974	1.667	1.000	3.338
2.50	11.0	6.248	-3.374	1.667	1.000	3.338
2.50	12.0	6.648	-2.774	1.667	1.000	3.338
2.50	13.0	7.048	-2.174	1.667	1.000	3.338

terpolation purposes one might take advantage of the following differential thermodynamic relations

$$d \ln \rho = \frac{1}{\Gamma_1} d \ln P - \delta \frac{ds}{c_p}, \quad (\text{B.1})$$

and

$$d \ln T = \nabla_{\text{ad}} d \ln P + \frac{ds}{c_p}. \quad (\text{B.2})$$

∇_{ad} is related to the thermodynamic derivatives given in Table B1 according to

$$\nabla_{\text{ad}} = \frac{P\delta}{\rho c_p T}. \quad (\text{B.3})$$

Appendix C: Fitting functions

The fits for s_{env} , entropy jump Δs , α_{MLT} , and α_{CMT} shown in Figs. 3, 4, 5, and 6 were computed from expressions (C.3), (C.4), and (C.5) (for α_{MLT} and α_{CMT}) in terms of the auxiliary

Table C.1. Coefficients for fitting functions

coefficient	s_{env}/s_0	$\Delta s/s_0$	α_{MLT}	α_{CMT}
a_0	1.6488	0.029	1.587	0.414
a_1	0.0740	0.166	-0.054	-0.100
a_2			0.045	-0.026
a_3	1.7860	1.225	-0.039	-0.065
a_4	-1.6762	-1.209	0.176	-0.092
a_5	0.1274	0.073	-0.067	0.193
a_6	-0.1412	-0.132	0.107	-0.125

variables \tilde{T} and \tilde{g} defined below. The coefficients a_i are listed in Table C.1. The fitting functions were generated automatically from a prescribed set of basis functions with the mere intention of providing numerical fits to the RHD data points which then allow the RHD results to be utilized easily in other contexts. Physical considerations did not enter, and we present the formulae in a form more suitable for computing rather than for human interpretation. We warn the reader that the fits quickly lose their meaning outside the region covered by the RHD model grid and should not be extrapolated too far.

$$\tilde{T} \equiv (T_{\text{eff}} - 5770)/1000 \quad (\text{C.1})$$

$$\tilde{g} \equiv \log(g/27500) \quad (\text{C.2})$$

$$\frac{s_{\text{env}}}{s_0} = a_0 + a_5\tilde{T} + a_6\tilde{g} + a_1 \exp[a_3\tilde{T} + a_4\tilde{g}] \quad (\text{C.3})$$

$$\frac{\Delta s}{s_0} = a_0 + a_1 \exp[(a_3 + a_5\tilde{T} + a_6\tilde{g})\tilde{T} + a_4\tilde{g}] \quad (\text{C.4})$$

$$\alpha = a_0 + (a_1 + (a_3 + a_5\tilde{T} + a_6\tilde{g})\tilde{T} + a_4\tilde{g})\tilde{T} + a_2\tilde{g} \quad (\text{C.5})$$

References

- Abbett W.P., Beaver M., Davids B., et al., 1997, ApJ 480, 395
 Alencar S.H.P., Vaz L.P.R., 1997, A&A 326, 257
 Antia H.M., 1996, A&A 307, 609
 Böhm-Vitense E., 1958, Zs. Ap. 46, 108
 Canuto V.M., Mazzitelli I., 1991, ApJ 370, 295
 Canuto V.M., Mazzitelli I., 1992, ApJ 389, 724
 Canuto V.M., Goldman I., Mazzitelli I., 1996, ApJ 473, 550
 Castellani V., Degl'Innocenti S., Marconi M., 1999, MNRAS 284, 265
 Chan K.-L., Sofia S., 1989, ApJ 336, 1022
 Christensen-Dalsgaard J., 1997, in: *Solar Convection and Oscillations and Their Relationship*, eds. F.P. Pijpers, J. Christensen-Dalsgaard, C.S. Rosenthal, Kluwer Academic Publisher, 3
 Cox J.P., Giuli R.T., *Principles of Stellar Structure*, Gordon and Breach, 1968
 Freytag B., Salaris M., 1999, ApJL, in press
 Freytag B., Ludwig H.-G., Steffen M., 1996, A&A 313, 497
 Henyey L., Vardya M.S., Bodenheimer P., 1965, ApJ 142, 841
 Kim Y.-C., Fox P.A., Sofia S., Demarque P., 1995, ApJ 442, 422
 Kurucz R.L., 1979, ApJS 40, 1
 Lucy L.B., 1967, Zs. f. Astrophys. 65, 89
 Ludwig H.-G., Jordan S., Steffen M., 1994, A&A 284, 105

- Ludwig H.-G., Freytag B., Steffen M., Wagenhuber J., 1996, in: *Stellar Evolution: What Should Be Done*, Proc. of the 32th Liège International Astrophysical Colloquium, eds. A. Noel et al., 213
 Ludwig H.-G., Freytag B., Steffen M., 1997, in: *Solar Convection and Oscillations and Their Relationship*, eds. F.P. Pijpers, J. Christensen-Dalsgaard, C.S. Rosenthal, Kluwer Academic Publisher, 59
 Lydon T.J., Fox P.A., Sofia S., 1992, ApJ 397, 701
 Lydon T.J., Fox P.A., Sofia S., 1993a, ApJL 403, 79
 Lydon T.J., Fox P.A., Sofia S., 1993b, ApJ 413, 390
 Mihalas D., *Stellar Atmospheres*, 2nd edition, Freeman and Company, 1978
 Nordlund Å., 1982, A&A 107, 1
 Nordlund Å., Dravins D., 1990, A&A 228, 155
 Nordlund Å., Spruit H.C., Ludwig H.-G., Trampedach R., 1997, A&A 328, 229
 Richard O., Vauclair S., Charbonnel C., Dziembowski W.A., 1996, A&A 312, 1000
 Rogers F.J., Iglesias C.A., 1992, ApJ 401, 361
 Rogers F.J., Swenson F.J., Iglesias C.A., 1996, ApJ 456, 902
 Spruit H.C., 1997, Mem. Soc. Astron. It. 68, 397
 Steffen M., 1993, in *Inside the stars*, IAU Colloquium 137, eds. W. Weiss, A. Baglin, Astron. Soc. Pacif. Conf. Series Vol. 40, p. 300
 Steffen M., Ludwig H.-G., 1999, in *Theory and tests of convective energy transport*, eds. A. Gimenez, E. Guinan, B. Montesinos, in press
 Steffen M., Ludwig H.-G., Krüß A., 1989, A&A 213, 371
 Steffen M., Ludwig H.-G., Freytag B., 1995, A&A 300, 473
 Stein R.F., Nordlund Å., 1989, ApJ 342, L95
 Trampedach R., Christensen-Dalsgaard J., Nordlund Å., Stein R.F., 1997, in: *Solar Convection and Oscillations and Their Relationship*, eds. F.P. Pijpers, J. Christensen-Dalsgaard, C.S. Rosenthal, Kluwer Academic Publisher, 73
 Unsöld A., *Physik der Sternatmosphären*, 2nd edition, Springer, 1955